JOC*Note*

Site Selectivity Switch in Lewis Acid Catalysis. Mechanism and Kinetic Simulation of Skeletal Rearrangement of Cyclobutene-Fused Homoquinones

Ken Kokubo, Takuya Koizumi, Kenji Harada, Eiko Mochizuki, and Takumi Oshima*

Division of Applied Chemistry, Graduate School of Engineering, Osaka University, Suita, Osaka 565-0871, Japan

oshima@chem.eng.osaka-u.ac.jp

Received July 7, 2005

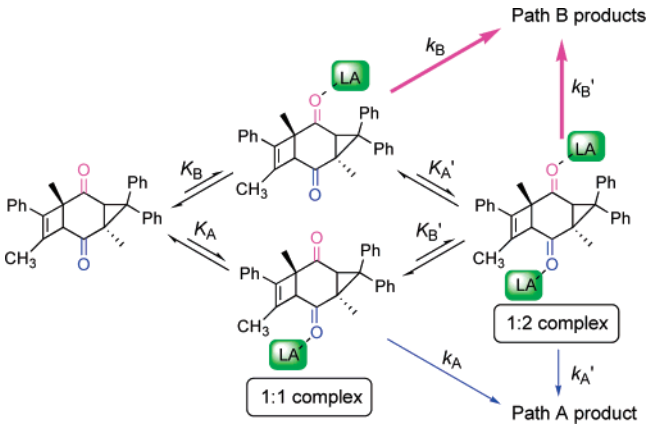

We investigated the site selectivity switch in BF_3-catalyzed dual skeletal rearrangements of cyclobutene-fused diarylhomobenzoquinones by changing the stoichiometric amount of acid concentration. From the lower to the higher equivalency of BF_3·Et_2O, the branching product ratios (path A/path B) obeyed nonlinear sigmoid curves against the equivalency of BF_3·Et_2O. The observed selectivity profiles were simulated to elucidate factors that govern thermodynamic aspects (binding affinity K of each carbonyl function with acid) and kinetic aspects (rate constants k for the cyclobutene-ring cleavage).

Lewis acids (LAs) are versatile catalysts in a variety of organic reactions, including additions, substitutions, isomerizations, and rearrangements. Continuous effort has been exerted to attain high chemo-, regio-, and stereoselectivity through modification of the catalyst.[1] If the substrate of interest possesses several acid-binding sites (i.e., basic lone-pair electrons) showing different reaction features, the preferential occurrence of the desired pathway requires appropriate control of the reaction conditions. However, such site selectivity control has been explored less than other selectivities.[2]

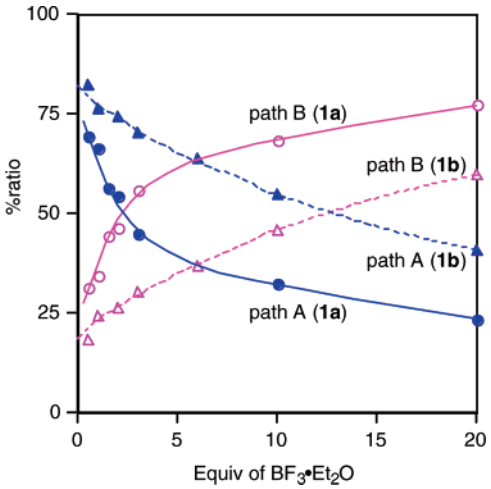

FIGURE 1. Plots of product ratios (%) of path B (open symbols) and path A (filled symbols) vs the equivalency of BF_3·Et_2O relative to substrate **1** (30 mM) on the rearrangement of **1a** (circles) and **1b** (triangles) catalyzed by BF_3·Et_2O at 25 °C in $CDCl_3$.

In previous papers, we have reported that the cyclobutene-fused homoquinone **1a**, which has two basic carbonyl sites and high strain energy, undergoes a two-way tandem skeletal rearrangement upon treatment with various Lewis acids to give several polycyclic ketones quantitatively[3] (Scheme 1). The kinetic substituent effects and solvent effects indicated that the reaction proceeds through a concerted S_N2-like mechanism involving a unique *endo*-aryl-assisted transition state.[4] In this paper, we wish to report interesting stoichiometric effects of the catalyst on site selectivity (selectivity switch) in the rearrangement of homoquinones **1a** and **1b**. Simulation of the observed selectivity profile also allows evaluation of the factors governing acid binding ability as well as the rate of the cyclobutene-ring cleavage.

Reaction of 1,5-dimethyl-substituted **1a** (30 mM) was carried out using various amounts of BF_3·Et_2O in $CDCl_3$ at 25 °C (±1 °C) for 1−100 h. Interestingly, however, the product branching ratio of **2** to **3** + **4** + **5** (path A/B) increased gradually with the increase of BF_3·Et_2O but decreased concomitant with a decrease in the catalyst, demonstrating a selectivity switch at ca. 2.5 equiv excess of the catalyst (solid lines, Figure 1). A similar selectivity change was also observed for 1,3-dimethyl-substituted **1b** (dotted lines), but the crossing (switching) point moved to the higher catalyst concentration (ca. 12.5 equiv). According to the mechanism depicted in Scheme 1, path B is kinetically preferred to path A because of the involvement of the tertiary carbocation intermediate **I**. However, the less hindered path A carbonyl benefits from stronger complexation with BF_3 as compared to the carbonyl of the hindered path B.[3b] Actually, the progress of each path can be related to the product of the

(1) Yamamoto, H. In *Lewis Acids in Organic Synthesis*; Yamamoto, H., Ed.; Wiley-VCH: Weinheim, Germany, 2000; p 1.
(2) For example: (a) Nagano, Y.; Orita, A.; Otera, J. *Bull. Chem. Soc. Jpn.* **2003**, *76*, 2183−2189. (b) Kobayashi, Y.; Kiyotsuka, Y. *Tetrahedron Lett.* **2001**, *42*, 9229−9232. (c) Nagatsuka, T.; Yamaguchi, S.; Totani, K.; Takao, K.; Tadano, K. *Synlett* **2001**, 481−484. (d) Mikami, K.; Terada, M.; Nakai, T. *J. Org. Chem.* **1991**, *56*, 5456−5459.
(3) (a) Kokubo, K.; Koizumi, T.; Oshima, T. *Tetrahedron Lett.* **2001**, *42*, 5025−5028. (b) Koizumi, T.; Mochizuki, E.; Kokubo, K.; Oshima, T. *J. Org. Chem.* **2004**, *69*, 4577−4585.
(4) Koizumi, T.; Harada, K.; Mochizuki, E.; Kokubo, K.; Oshima, T. *Org. Lett.* **2004**, *6*, 4081−4084.

10.1021/jo051399i CCC: $30.25
Published on Web 08/24/2005

SCHEME 1. Lewis Acid Catalyzed Dual Skeletal Rearrangement of the Cyclobutene-Fused Homoquinone 1

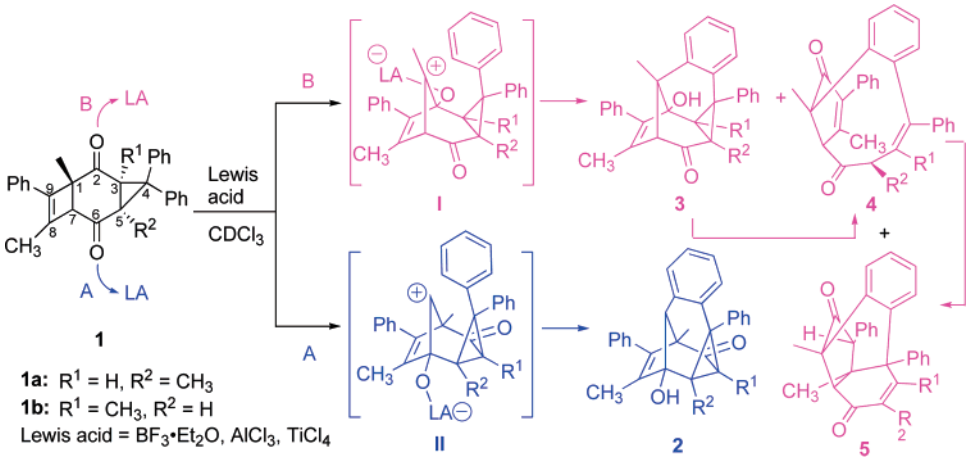

SCHEME 2. Kinetic and Thermodynamic Scheme for the BF_3·Et_2O-Catalyzed Skeletal Rearrangement of 1

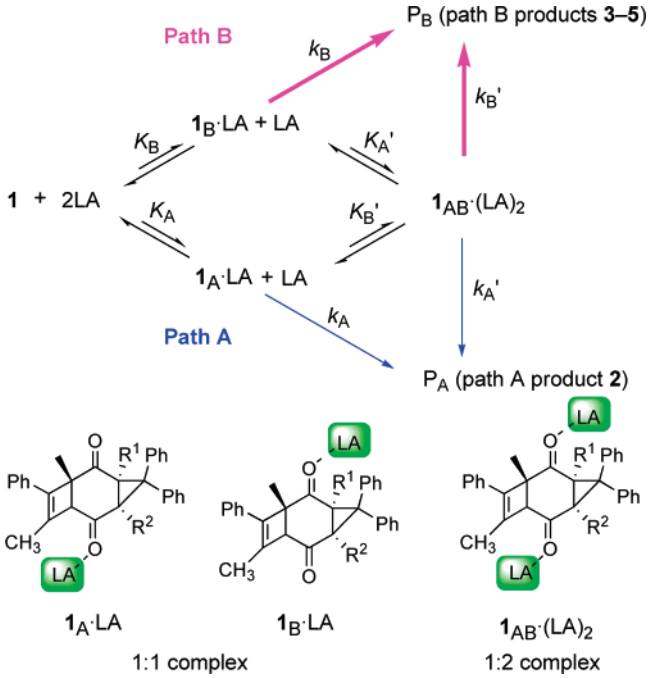

complexation affinity K of each carbonyl group and the rate constant k for the initial vinyl migration.[5] The observed selectivity switch can only be explained by formation of the carbonyl-bound 1:2 complex $\mathbf{1}_{AB}$·$(LA)_2$ on increasing LA (=BF_3).

Scheme 2 shows that because the 1:2 complex $\mathbf{1}_{AB}$·$(LA)_2$ participates in the rearrangement of **1**, the proportion of the kinetically favored path B is raised, where K, k, and P respectively indicate the binding constants with BF_3, the rate constants for the initial 1,2-vinyl migration, and the products. Subscripts A and B refer respectively to paths A and B.

The formation rate for P_A (**2**) can be expressed as eq 1:

$$\frac{dP_A}{dt} = k_A[\mathbf{1}_A\cdot LA] + k_A'\,[\mathbf{1}_{AB}\cdot(LA)_2] \qquad (1)$$

Using K_A and K_B', eq 1 can be rewritten as eq 2:

$$\frac{dP_A}{dt} = K_A[\mathbf{1}][LA](k_A + k_A'K_B'[LA]) \qquad (2)$$

With a similar equation for formation of P_B (**3**−**5**), the product ratio of path A/B is expressed as eq 3:

$$\frac{P_A}{P_B} = \frac{K_A(k_A + k_A'K_B'[LA])}{K_B(k_B + k_B'K_A'[LA])} \qquad (3)$$

Assuming that the rate constants k and binding constants K are almost identical for each pathway irrespective of the stoichiometric difference of BF_3 complexes, i.e., $k_A \cong k_A'$, $k_B \cong k_B'$, $K_A \cong K_A'$, and $K_B \cong K_B'$, eq 3 may be simplified as eq 4:

$$\frac{P_A}{P_B} = \frac{k_AK_A(1 + K_B[LA])}{k_BK_B(1 + K_A[LA])} \qquad (4)$$

Apparently, the product ratio P_A/P_B converges asymptotically to the ratio of k_AK_A/k_BK_B at lower catalyst concentration ($1 \gg K[LA]$) and oppositely to the rate ratio k_A/k_B at higher concentration ($1 \ll K[LA]$). Actually, the product ratios obtained in a wide range of practical catalyst concentration (0.02−264 equiv (neat)) showed characteristic sigmoid curves for both **1a** and **1b**, consistent with the previous argument (Figure 2).

Table 1 presents a summary of the estimated values of k and K from the curve-fitting simulation[6] along with the observed second-order rate constant k_{obs} at the lower catalyst concentration. Values of k_AK_A and k_BK_B are calculated[7,8] using curve-fitting methods from experi-

(5) Study of stoichiometric complexation: Hunt, I. R.; Rogers, C.; Woo, S.; Rauk, A.; Keay, B. A. *J. Am. Chem. Soc.* **1995**, *117*, 1049−1056.

(6) The curve-fitting simulation of eq 4 with experimental values was carried out using the Solver program of Microsoft Excel software (least-squares method).

(7) [LA] in eq 4 includes the complexation equilibrium between BF_3 and Et_2O. However, [Et_2O] is omitted for simplification.

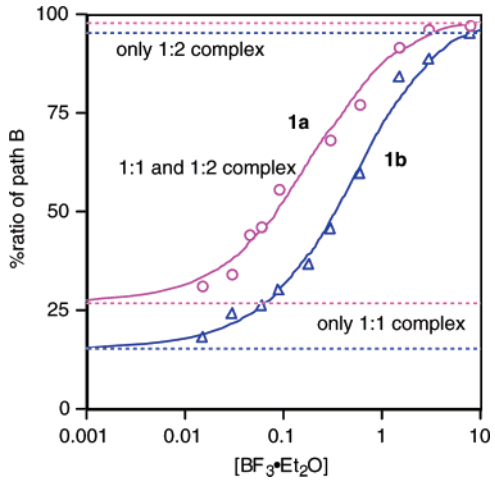

FIGURE 2. Plots of path B product ratios (%) for rearrangement of **1a** (circles) and **1b** (triangles) vs BF_3·Et_2O concentration (on a logarithmic scale). Each calculated fitting curve is shown as a solid line. Dotted lines show asymptotes corresponding to the extreme case of only the presence of a 1:1 or 1:2 complex.

TABLE 1. Estimated Kinetic Parameters

	1a	1b
k_A/k_B[a]	0.031 (3:97)[b]	0.053 (5:95)[b]
k_AK_A/k_BK_B[a]	2.23 (69:31)[c]	4.59 (82:18)[c]
K_A/K_B	72.0	87.1
k_AK_A	2.24×10^{-3}	1.34×10^{-3}
k_BK_B	8.81×10^{-4}	3.05×10^{-4}
$k_AK_A + k_BK_B$	3.12×10^{-3}	1.64×10^{-3}
k_{obs}[d]	2.65×10^{-3}	9.66×10^{-4}

[a] Values obtained from experimental data of P_A/P_B. [b] The ratio in parentheses is P_A:P_B at 264 equiv of BF_3·Et_2O (neat). [c] P_A:P_B at 0.5 equiv of BF_3·Et_2O. [d] Obtained by dividing the pseudo-first-order rate constant with BF_3·Et_2O concentration that was used (3 equiv).

mental values of k_A/k_B and k_AK_A/k_BK_B. The simulation validity is demonstrated by the reasonable agreement of k_{obs} with $k_AK_A + k_BK_B$ (Table 1).

Moreover, the estimated values were in good agreement with the switching profile of experimental results. Rate constants k_A in both **1a** and **1b** are 1/30- to 1/20-fold smaller than k_B, reflecting the stability difference between intermediates **I** and **II**. However, the binding constants K_A are 70−90 times larger than K_B. Thus, at lower concentration of BF_3·Et_2O, in which the 1:1 complex dominates the kinetics, the binding constant is so important that the reaction rate is proportional to the product of k and K. On the other hand, for higher concentrations of BF_3·Et_2O, in which the 1:2 complex dominates the kinetics, the binding constant is less important and the rate is only proportional to the rate constant k. The site selectivity switch is thus explained reasonably by assuming that path B is favored by the higher rate constant k_B but has the disadvantage of the reduced binding constant K_B caused by steric hindrance of the adjacent methyl groups. The value of $K_A/K_B > 1$ in both **1a** and **1b** indicates that steric hindrance from the methyl group is more serious in the cyclobutene-side methyl group than in the cyclopropane-side one.[9] The larger value of K_A/K_B for **1b** (87.1) as compared to that for **1a** (72.0) is reasonable, because path B of **1b** engenders greater steric hindrance with both two methyl groups. Therefore, the shift of the crossing point of **1b** to the higher BF_3 concentration is attributable to the more enhanced steric hindrance around the C2 carbonyl site as compared to that of the C6 carbonyl.

In conclusion, we found the site selectivity switch in the Lewis acid catalyzed dual rearrangement of cyclobutene-fused homoquinones **1** because of the higher order complexation. Consequently, thermodynamic and kinetic balances on each reaction pathway explained nonlinear stoichiometric effects of the catalyst on product distributions. These findings provide useful insights into the fields of synthetic and theoretical organic chemistry.

Experimental Section

Cyclobutene-fused homobenzoquinones **1a**,**b** were synthesized by the [2 + 2] photocycloaddition of the corresponding homobenzoquinone with alkynes as previously described.[10] The rearrangement products were isolated by HPLC equipped with a semifractionation ODS column and recrystallized from hexane−benzene. The compounds **1a**, **2a**, **4a**, and **5a** were already reported (**3a** was not formed).[3] The new compounds **1b**, **2b**, **3b**, and **5b** were identified by ^1H and ^{13}C NMR as well as IR spectra as follows (**4b** was not formed), and also the structures of **3b** (CCDC 279749) and **5b** (CCDC 279750) were confirmed by X-ray crystallographic analysis.

General Procedure for BF_3·Et_2O-Catalyzed Reactions of 1. BF_3·Et_2O (7.6 μL, 0.06 mmol) was added into a $CDCl_3$ solution (670 μL) of **1a** (8.36 mg, 0.02 mmol) in a NMR tube using a microsyringe at room temperature. The progress of the reaction was monitored by ^1H NMR. After a requisite period of time, the reaction solution was transferred into a separate funnel, diluted with chloroform (10 mL), and then washed with water (3 mL × 3). The aqueous layer was extracted with chloroform (5 mL × 2). The combined organic layers were washed with water (3 mL × 3) and then dried over calcium chloride. After the evaporation of the solvent, the residue was submitted for a ^1H NMR analysis to determine the product distribution.

(1*R,3*R**,5*R**,7*R**)-1,3,8-Trimethyl-4,4,9-triphenyltricyclo-[5.2.0.0^{3,5}]non-8-ene-2,6-dione (1b):** mp 162.2−163.0 °C; white crystal; ^1H NMR (270 MHz, $CDCl_3$) δ 0.75 (s, 3H), 1.16 (s, 3H), 2.02 (d, 3H, J = 1.6 Hz), 2.54 (d, 1H, J = 1.6 Hz), 2.73 (s, 1H), 7.17−7.51 (m, 15H); ^{13}C NMR (67.5 MHz, $CDCl_3$) δ 14.2, 18.8, 19.5, 40.1, 42.8, 47.1, 56.0, 61.3, 136.6, 127.2, 127.65, 127.69, 128.3, 128.65, 128.74, 128.9, 130.3, 132.6, 138.3, 138.4, 141.0, 143.7, 204.1, 208.1; IR (KBr) 1672 (C=O) cm^{-1}. Anal. Calcd for $C_{30}H_{26}O_2$: C, 86.09; H, 6.26. Found: C, 86.28; H, 6.41.

(1*S,2*S**,9*S**,10*R**,13*S**,14*R**)-13-Hydroxy-1,10,12-trimethyl-2,11-diphenylpentacyclo[8.4.1.0^{2,14}.0^{3,8}.0^{9,13}]pentadeca-3(8),4,6,11-tetraen-15-one (2b):** white crystal; ^1H NMR (270 MHz, $CDCl_3$) δ 1.03 (s, 3H), 1.12 (s, 3H), 1.93 (s, 1H), 2.01 (s, 3H), 2.52 (d, 1H, J = 2.6 Hz), 3.53 (d, 1H, J = 2.6 Hz), 6.89 (dd, 1H, J = 6.9, 2.0 Hz), 7.06−7.52 (m, 13H); ^{13}C NMR (67.5 MHz, $CDCl_3$) δ 11.5, 15.1 20.0, 38.9, 43.6, 48.1, 63.1, 68.6, 75.9, 126.0, 127.1, 127.5, 127.6, 127.7, 128.0, 128.1, 128.3, 129.4, 130.0, 130.2, 131.3, 132.3, 135.3, 137.1, 138.3, 139.2, 147.2, 205.0.

(8) Reaction of **1a** with 3 equiv of BF_3·Et_2O reveals that the product branching ratio remains within 60 ± 1.2% during the reaction. This result indicates that the products have binding affinities similar to that of the substrate and do not change the concentration of [LA].

(9) However, the dihedral angles between the methyl group and the adjacent carbonyl group of **1a** are 48.3° on the cyclobutene side and 26.5° on the cyclopropane side, respectively, determined by X-ray crystallography.[3b] Thus, the reason for the greater steric hindrance from the methyl group on the cyclobutene side as compared to that on the cyclopropane side may be due to the additional contribution of a phenyl group to the cyclobutene ring.

(10) Kokubo, K.; Yamaguchi, H.; Kawamoto, T.; Oshima, T. *J. Am. Chem. Soc.* **2002**, *124*, 8912−8921.

(1*S,2*R**,9*S**,10*S**,13*S**,14*S**)-13-Hydroxy-9,11,14-trimethyl-2,12-diphenylpentacyclo[8.4.1.0^{2,14}.0^{3,8}.0^{9,13}]pentadeca-3(8),4,6,11-tetraen-15-one (3b):** mp 285.5−286.5 °C; white crystal; ^{1}H NMR (270 MHz, $CDCl_3$) δ 0.78 (s, 3H), 1.80 (s, 1H), 1.83 (s, 3H), 1.87 (s, 3H), 2.47 (d, 1H, J = 1.0 Hz), 2.89 (s, 1H), 6.56 (dd, 1H, J = 1.0, 8.2 Hz), 7.04−7.56 (m, 13H); ^{13}C NMR (67.5 MHz, $CDCl_3$) δ 14.7, 16.3, 19.1, 42.3, 43.3, 51.7, 54.0, 75.9, 82.8, 126.3, 126.8, 126.9, 127.3, 127.4, 128.2, 128.4, 128.5, 128.8, 129.1, 130.6, 131.1, 135.7, 135.9, 137.7, 139.1, 146.3, 200.7; IR (KBr): 3480 (br, OH), 1668 (C=O) cm^{-1}.

(2*S,4*R**,5*R**,6*R**,10*R**)-2,5,9-Trimethyl-4,10-diphenyltetracyclo[9.4.0.0^{2,6}.0^{5,10}]pentadeca-1(15),8,11,13-tetraene-3,7-dione (5b):** white crystal; ^{1}H NMR (270 MHz, $CDCl_3$) δ 1.66 (s, 3H), 1.75 (s, 3H), 1.80 (d, 3H, J = 1.0 Hz), 2.77 (s, 1H), 3.65 (s, 1H), 6.13 (q, 1H, J = 1.0 Hz), 6.13−6.34 (m, 4H), 6.88−7.46 (m, 9H); ^{13}C NMR (67.5 MHz, $CDCl_3$) δ 17.0, 21.9, 27.2, 49.9, 56.9, 59.0, 63.4, 66.2, 125.4, 125.5, 125.9, 126.7, 127.1, 127.90, 127.93, 128.4, 128.69, 129.74, 129.9, 130.7, 132.6, 132.8, 134.2, 134.8, 138.2, 168.9, 194.1, 206.7.

X-ray Crystal Structure Determination of 3b: $C_{30}H_{26}O_2$, M_r = 418.53, monoclinic, space group $P2_1/c$, with a = 12.752(7) Å, b = 13.44(1) Å, c = 14.274(4) Å, β = 115.22(3)°, V = 2213.46 Å^3, Z = 4, D_c = 1.256 g/cm^3, R = 0.079 and R_w = 0.079 for 3380 reflections with $I > 3.00\sigma(I)$.

X-ray Crystal Structure Determination of 5b: $C_{30}H_{26}O_2$, M_r = 418.53, monoclinic, space group $P2_1/c$, with a = 15.503(5) Å, b = 8.505(2) Å, c = 16.954(3) Å, β = 100.37(2)°, V = 2199.0(9) Å^3, Z = 4, D_c = 1.264 g/cm^3, R = 0.070 and R_w = 0.054 for 2657 reflections with $I > 3.00\sigma(I)$.

Kinetic Simulation for BF_3·Et_2O-Catalyzed Reactions of 1. The theoretical product ratio P_A/P_B for each concentration of BF_3·Et_2O was calculated by eq 4. The estimated kinetic parameters were obtained by using the program Solver in Microsoft Excel software, reducing the difference between calculated and experimental values of P_A/P_B on the basis of the least-squares method.

Acknowledgment. This work was financially supported by the General Sekiyu Research and Development Encouragement and Assistance Foundation.

Supporting Information Available: Text giving detailed experimental procedures, tables showing the product distribution, and CIF files giving crystallographic data for compounds **3b** and **5b**. This material is available free of charge via the Internet at http://pubs.acs.org.

JO051399I